Hindawi
Advances in Civil Engineering
Volume 2020, Article ID 8839386, 11 pages
https://doi.org/10.1155/2020/8839386

Research Article

Research on the Corrosion Damage Mechanism of Concrete in Two Freeze–Thaw Environments

Xianhua Yao,[1] Min Zhang,[1] Junfeng Guan ,[1] Lielie Li ,[1] Weifeng Bai,[2] and Zepeng Liu[1]

[1]*School of Civil Engineering and Communication, North China University of Water Resources and Electric Power, Zhengzhou 450045, China*
[2]*School of Water Conservancy, North China University of Water Resources and Electric Power, Zhengzhou 450045, China*

Correspondence should be addressed to Junfeng Guan; shuaipipi88@126.com and Lielie Li; 13370912@qq.com

Received 21 August 2020; Revised 13 September 2020; Accepted 21 September 2020; Published 8 October 2020

Academic Editor: Yifeng Ling

This study aims to investigate the effects of two freeze–thaw environments (i.e., maintenance freeze-thaw (MFT) environment and immersion freeze-thaw (IFT) environment) on the durability performance, deterioration rules, and mechanisms of concrete. In MFT, the concrete specimens were firstly cured in the standard curing environment (temperature, 20 ± 3, humidity, not less than 95%, and ages, 28 d) and then were carried out in freeze–thaw environment, while in IFT, the concrete specimens were firstly cured in the salt ($NaHCO_3$, NaCl, and Na_2SO_4) immersion environment for 90 d and then were carried out in freeze–thaw environment. In this study, the damage features, relative dynamic elastic modulus, mass changes, and erosion-resistance coefficient of concrete have been measured. Thereafter, using the scanning electron microscopy (SEM) and the mercury intrusion porosimetry (MIP), the air-void structure parameters and the microstructures have been measured, respectively. The results show that the relative dynamic elastic modulus and the erosion-resistance coefficient of the compressive strength of the concrete in the IFT environment are, respectively, 14.3% and 21.0% higher than those of the concrete in the MFT environment. In addition, the results of the microstructure analyses show that the corrosion damages of the concrete are mainly caused by the combined action of the corrosion products of ettringite and freeze–thaw environment. However, the damage to the concrete in the MFT environment is more serious than that in the IFT environment. The results of the MIP analysis show that the harmful pore value for the concrete in the MFT environment is almost two times larger than that for the concrete in the IFT environment.

1. Introduction

Many earlier studies investigated the damage to concrete caused by freeze-thaw cycles [1, 2]. Ma et al. [3] showed that the frost resistance of high-performance concrete blended with 20 wt% fly ash (FA) and 0.1% polypropylene fiber was superior when subjected to rapid freeze-thaw cycles. Zhou and Qiao [4] observed that when a concrete material was subjected to rapidly repeated freeze-thaw cycles, the energy-based approach was more sensitive and effective than the elastic modulus-based approach in evaluating the deterioration of the concrete material over time and capturing the accumulative material degradation. Liu et al. [5] found that the addition of FA in ordinary concrete reduced the formation of gypsum and prevented the decalcification of calcium silicate hydrate (C-S-H) when subjected to sodium sulfate attack. Zhang et al. [6] found that an excessive number of nano-SiO2 particles could have an adverse effect on the durability of the concrete. Forgeron [7] and Trottier [8] found that the mechanical properties of concrete under the combined action of the fatigue load and the freeze-thaw cycles were equivalent or even better than when only the fatigue load was applied. Diao et al. [9] reported that with the increase in the number of freeze-thaw cycles, the compressive strength of concrete decreased when subjected to alternating actions of the freeze-thaw cycles and seawater immersion. Gong et al. [10] developed a comprehensive hydraulic pressure model that can be applied to different cases, such as different saturation degrees and cooling rates. Diao et al. [11] found that when subjected to the freeze-thaw

cycles and mixed corrosion, the loading capacity of reinforced concrete beams decreased by 4%. Amini and Tehrani [12] developed quantitative damage models to predict the mass loss and the compressive strength loss due to the combined effect of saltwater and water flow on the deterioration of concrete subjected to freeze-thaw cycles. Richardson et al. [13] found that rubber crumb was effective in providing freeze-thaw protection. Yuan et al. [14] observed that the extent of concrete damage increased gradually from surface to complete disintegration of the interior concrete after 30 freeze-thaw cycles. Wang et al. [15] found that the freezing temperature was independent of the freeze-thaw cycles; however, thawing temperature changed with the number of freeze-thaw cycles. Shang et al. [16] found that the loss of the compressive strength and the tensile strength of concrete was more evident than those of the dynamic modulus of elasticity and the weight loss after the concrete was subjected to the freeze-thaw cycles. Ranz et al. [17] developed a nondestructive methodology that can be used as an alternative method to evaluate the damage in cementitious materials when subjected to freeze-thaw cycles. Li et al. [18] found that air content can delay the time for concrete to reach a critical degree of saturation; however, this did not prevent the damage to concrete caused by the freeze-thaw cycles. Richardson et al. [19] observed that fibers had the ability to entrain air, which might contribute to the improvement in freeze-thaw durability. Zhang et al. [20–22] showed that nano-SiO_2, nano-$CaCO_3$, and ground-granulated blast-furnace slag could strengthen mechanical performance of concrete. Li et al. [23] found that the deterioration of concrete under the freeze-thaw plus dry-wet conditions was significantly higher than that under the dry-wet plus freeze-thaw conditions and much higher than that under one of these two conditions only. Su and Wang [24] studied the corrosion damage properties of concrete subjected to multi-salt soaking, freeze-thaw, and dry-wet cycles. Yao et al. [25, 26] investigated the microscopic mechanism of concrete using multiple admixtures under the common action of multisalt soaking, wetting-drying, and freeze-thaw cycles.

Researchers have also carried out studies on the influences of different freeze–thaw environments on concrete. Shi et al. [27] found that with the increase in the freeze–thaw cycles the concrete elastic moduli at the upper-limit temperature were decreasing due to the accumulated damage caused by the freeze–thaw cycle action of different temperature ranges. Under different freeze–thaw media, Yin et al. [28] showed that the concrete in 3.5wt% NaCl solution was much worse than that in water, and the degree of deterioration of the mass loss rate, relative dynamic elastic modulus, average compressive strength, and porosity of CT scanning images of the recycled aggregate pervious concrete increased with the increasing number of freeze–thaw cycles. In the investigation of the difference between the effects of the water-resistant freeze–thaw and the salt–freeze–thaw cycles on ordinary concrete, Xu et al. [29] found that there was a multiplier relationship between the two, and the multiplier value had nothing to do with the concrete mix ratio, strength grade, and stone powder content. By analyzing the mechanical properties of concrete subjected to freeze–thaw cycles in three solutions (i.e., water, 3.5 wt% NaCl, and aircraft deicing fluid), Zhao et al. [30] found that the damage to the concrete in 3.5 wt% NaCl solution was much worse than that in water, and there was only limited damage to the concrete in the aircraft deicing fluid. Through a study of the effects of different freezing and thawing methods on the fracture of concrete with double-k, Hu et al. [31] found that there were similarities in the influence of different freeze–thaw methods on the concrete.

However, most of these earlier studies focused on the damage to concrete under a water freeze-thaw environment or a sulfate attack environment. Even for the studies on the effects of different freeze–thaw environments on the mechanical properties and microstructures of concrete, the methods used in most of these studies were freezing and thawing concrete in water, or in a single salt (e.g., NaCl) solution. They did not investigate freezing and thawing concrete in a multisalt (NaCl, Na_2SO_4, and $NaHCO_3$) solution. Therefore, it is necessary to investigate the durability performance and deterioration rules and mechanisms of concrete in different freeze–thaw environments, including the multisalt freeze–thaw environments.

In real-life practical engineering, the corrosive failure mechanisms of concrete are different in different parts of China. For instance, in the cold saline-alkali corrosive areas in Western China, concrete may encounter two situations. One is for the concrete to be subjected to the composite salt freeze-thaw cycles after a certain standard curing period (usually not more than 28 days and the concrete specimens were in water only). The other is for the concrete to be subjected to the multisalt freeze-thaw cycles after a certain period of erosion (generally 1–5 months and the concrete specimens were in the multisalt solution) caused by the multisalt (e.g., NaCl, Na_2SO_4, and $NaHCO_3$) [32]. In real-life practical engineering, the corrosive failure mechanism of concrete is different in the two situations above. However, there are only a few reports on the physical properties, chemical changes, mechanical performances, and microcrack evolution process of concrete subjected to freeze-thaw cycles and multisalt solution attack. Therefore, in the cold and saline-alkali corrosive areas of Western China, a study on the effects of freeze-thaw cycles and multisalt erosion on concrete has important scientific research significance and practical engineering value.

In this study, in view of the multisalt solution attack environment in the cold region in western China and the actual situation of Dexiang Expressway Project in Delingha City, Qinghai Province, the effects of two freeze-thaw environments (i.e., MFT and IFT) on the durability performance, deterioration rules, and mechanisms of concrete have been investigated using the concrete mix ratio provided by the site so as to develop theories for the actual project and experimental basis.

2. Experimental Materials and Concrete Specimens

2.1. Materials. In this study, PO 42.5 portland cement (provided by Qinghai Province Cement Co., Ltd, China) has

been used for the preparation of the concrete specimens. The concrete specimens have been prepared by replacing a part of FA (provided by Qinghai Province Datong Co., Ltd., China) and slag (provided by Qinghai Province Jintuo Co., Ltd., China). The chemical composition, physical and mechanical properties, and mineral compositions of the materials used are shown in Tables 1–5.

The reactive sand used in this study has the mud concentration of 0.8%, apparent density of 2650 kg/m^3, bulk density of 1470 kg/m^3, and fineness modulus of 2.6. The sand, provided by the manufacturer Qinghai Province, China, has been classified as a type of medium sand. The coarse aggregate used in this study was provided by the manufacturer Qinghai Province, China, has a continuous grade of 5–20 mm, the apparent density of 2520 kg/m^3, and bulk density of 1350 kg/m^3. The high-range water reducer used in this study was produced by Shanxi Province Chemical Co., Ltd. It has a naphthalene-type superplasticizer with a water reduction of greater than 20%. The content of Na_2SO_4 was less than 2%, and the content of chloride ions in water was less than 0.01%.

2.2. Concrete Specimens. The environment of the Dexiang Highway Project is a corrosive salt marsh environment. The salt marsh contains many types of corrosive ions (i.e., Cl^-, HCO_3^-, and SO_4^{2-}), which affect the durability of concrete negatively. Therefore, the soil samples in the area have been analyzed chemically. The artificial multi-salt consists of $NaHCO_3$, NaCl, Na_2SO_4, and H_2O, and the chemical reagents proportions are shown in Table 6. The mix proportion for the concrete specimens has been designed according to the practical engineering requirements of concrete. The mix proportion is shown in Table 7.

Then, the materials, such as cement, FA, SG, sand, gravel, and water-reducing agent, were dry mixed in a blender for 1 min. Thereafter, water was added, and the mixture was blended for 3 min. The concrete specimens of two sizes (100 mm × 100 mm × 100 mm and 100 mm × 100 mm × 400 mm) were produced. The 100 mm concrete cubes were used to measure the reduction in compressive strength and concrete mass and 100 mm × 100 mm × 400 mm prisms were used to measure the relative dynamic elastic modulus and microstructure. Each concrete specimen was placed in a mold and cured for 24 h. The concrete specimens were then divided into two groups. After demolding, one group was placed into water of (20 ± 3)°C for 28 d standard curing. The other group, also demolded, was placed into multisalt water for 90 d curing.

2.3. Experimental Program. In general, the damage mechanism and the reaction outcomes of concrete subjected to freeze-thaw cycles and multisalt solution attack are different. The internal structure of the concrete tends to be denser after the multisalt solution attack, as compared to the concrete after being subjected to the freeze-thaw cycles. Therefore, in order to investigate this difference, experiments have been carried out with the concrete specimens in the MFT and IFT environments, and the results are shown in experiment in the MFT environment and experiment in the IFT environment.

Table 1: Chemical composition of main raw materials (in percentage).

Material	SiO_2	Al_2O_3	Fe_2O_3	CaO	MgO	Na_2O	K_2O
PO 42.5	23.46	3.88	3.32	66.82	1.32	0.42	0.78
FA	55.31	26.83	5.65	5.88	2.56	1.98	1.79
Slag	47.33	6.43	1.12	40.23	3.21	0.77	0.91

Experiment in the MFT Environment. After immersing the concrete specimens in pure water of (20 ± 3)°C for 24 days, the specimens were immersed in the multisalt solution of (20 ± 3)°C for 4 days and subjected to 150 freeze-thaw cycles and multisalt solution attack. The mass change, compressive strength, and relative dynamic elastic modulus of the concrete specimens have been determined at 0, 25, 50, 75, 100, 125, and 150 cycles. Using the scanning electron microscopy (SEM) and mercury intrusion porosimetry (MIP), the microstructure of the concrete has been evaluated.

Experiment in the IFT Environment. This group of concrete specimens was exposed to the multisalt solution for 90 days and then subjected to 150 freeze-thaw cycles and multisalt solution attack. The mass change, compressive strength, and relative dynamic elastic modulus of concrete specimens have been determined at 0, 25, 50, 75, 100, 125, and 150 cycles. Using the scanning electron microscopy (SEM) and mercury intrusion porosimetry (MIP), the microstructure of the concrete has been evaluated.

In this study, the Standard for Test Methods of Long-Term Performance and Durability of Ordinary Concrete (GB/T 50082-2009) has been used as a guide. The concrete specimens of the sizes 100 mm × 100 mm × 100 mm and 100 mm × 100 mm × 400 mm have been prepared for the freeze-thaw test. During the test, the central temperature of the specimens was controlled, and they were changed between −15 ± 2°C and 6 ± 2°C. The deicer solution level was 20 mm higher than the top of the specimens. Each freeze-thaw cycle lasted for nearly 2 h, and the thawing time was approximately 2 h. The freeze-thaw test was stopped when the mass loss (W_n) reached 5% or the relative dynamic elastic modulus (E_r) decreased to 60%. At that point, the number of freeze-thaw cycles is considered as the maximum number of freeze-thaw cycles, n. The mass loss, W_n, is then calculated after n freeze-thaw cycles as follows:

$$W_n = \frac{G_0 - G_n}{G_0} \times 100\%, \quad (1)$$

where (G_0) is the original mass before the start of the freeze-thaw cycles, and (G_n) is the mass after n freeze-thaw cycles.

The relative dynamic elastic modulus, E_r, is calculated as follows:

$$E_r = \frac{E_n}{E_0} = \frac{f_n^2}{f_0^2} \times 100\% E_r, \quad (2)$$

where E_0 is the original relative dynamic elastic modulus of the concrete specimens, E_n is the relative dynamic elastic

Table 2: Basic physical and mechanical properties of cement.

Cement	Specific surface area ($m^2 \cdot kg^{-1}$)	Initial setting time	Final setting time	Compression strength (MPa)	
		Min	Min	3 d	28
PO 42.5	344	240	315	24.1	49.3

Table 3: Mineral composition of main raw materials (in percentage).

Material	C3S	C2S	C3A	C4AF	f-CaO
PO 42.5	55.7	22.09	5.12	16.79	0.29

Table 4: Basic physical and mechanical properties of FA (in percentage).

Material	Fineness (45 μm)	Water demand ratio	SO_3	Loss
FA	10.8	94	0.67	1.66

modulus of the concrete specimens after n freeze-thaw cycles, f_0^2 is the original frequency of the concrete specimens, and f_n^2 is the frequency of the concrete specimens after n freeze-thaw cycles. Further, the compression strength of the concrete specimens has been evaluated.

The erosion-resistance coefficient, K_c, of the specimens can be calculated as follows:

$$K_c = \frac{f_c}{f_s}, \tag{3}$$

where f_c is the compression strength of the concrete specimens subjected to n freeze-thaw cycles and the multisalt solution attack, and f_s is the original compression strength of the concrete specimens immersed in the multisalt solution before the start of the freeze-thaw cycles.

3. Experimental Results and Discussion

3.1. Visual Inspection. As shown in Figures 1 and 2 and Table 8, the degree of damage of the concrete specimens after being subjected to freeze-thaw cycles is different in different experiments. With the increase in the number of freeze-thaw cycles, the degree of damage of concrete increases gradually. After being subjected to the maximum number of freeze-thaw cycles in the IFT environment, which is 125, a large number of stones in the concrete specimen are exposed or at one end of the concrete specimen, they are even peeled. Comparing to that in the IFT environment, the damage of the concrete specimens in the MFT environment is more serious. The whole surface of the concrete specimen fell off. Moreover, when the number of freeze-thaw cycles reaches 100 times, the degree of damage of the concrete specimen is 125 times of that in the IFT environment. This is an indication that the MFT environment is more destructive to concrete than the IFT environment.

3.2. Mass Change. Figure 3 shows that the mass loss of the concrete specimen increases with increasing the number of freeze-thaw cycles. Before 75 freeze-thaw cycles, the mass loss of the concrete specimen in the IFT environment is slightly higher than that in the MFT environment. However, after 75 freeze-thaw cycles, due to the peeling of the concrete specimen in the MFT environment, the mass loss of the concrete specimen in the MFT environment is higher than that in the IFT environment. This is an indication that the rate mass loss of the concrete specimen in the MFT environment is faster after 75 freeze-thaw cycles.

3.3. Relative Dynamic Elastic Modulus. Figure 4 shows the variations of E_r of the concrete specimens subjected to the freeze-thaw cycles and the multisalt solution attack. Before 75 freeze–thaw cycles, E_r of the concrete specimen in the MFT environment is slightly higher than that in the IFT environment. That is to say, the MFT case showed better frost resistance in the first several cycles the IFT. However, the results show that in the latter stage of the concrete degradation, the decrease in E_r in the MFT environment is significantly larger than that in the IFT environment. This is an indication that the deterioration of concrete subjected to freeze-thaw cycles and the multisalt solution attack is faster due to the salt crystallization. For instance, in Figure 4, E_r for the concrete specimens in the MFT environment decreases by 48.7% after 100 freeze-thaw cycles. On the other hand, E_r for the concrete specimens in the IFT environment decreases by 44.2% after 125 freeze-thaw cycles. Hence, E_r for the concrete specimen in the MFT environment decreases by 4.5% more than that in the IFT environment. From the downward trend (Figure 4), when the number of freeze-thaw cycles increases from 75 to 100, E_r of the concrete specimen in the MFT environment decreases from 87.6% to 51.3% (a decrease of 36.3%). This sharp downward trend is an indication of brittle damage characteristics. By contrast, when the freeze-thaw cycles increases from 75 to 100, E_r of the concrete specimen in the IFT environment decreases from 75.7% to 61.4% (a decrease of 14.3%). So, the decrease in E_r of the concrete specimen in the IFT environment is slower than that in the MFT environment. Comparing with the damage caused by the freeze-thaw cycles, the damage to the concrete specimen by the salt solution attack is less. Therefore, the damage to concrete in the IFT environment is generally less than that in the MFT environment.

3.4. Erosion-Resistance Coefficients. Figure 5 shows the variations of K_c of the concrete specimens subjected to the freeze-thaw cycles and the multisalt solution attack. As shown in the figure, for the concrete specimens in the MFT environment, there is slight corrosion. In the initial stage, K_c of the concrete specimen increases with increasing the number of freeze–thaw cycles, which is known as the

Table 5: Basic physical properties of slag (in percentage).

Material	Specific surface area ($m^2 \cdot kg^{-1}$)	Loss	SO_3	Water demand ratio	Activity index	
					7 d	28 d
Slag	405	0.17	0.11	97	76	103

Table 6: Proportion of chemical reagents in multisalt. Unit: g/L.

$NaHCO_3$	NaCl	Na_2SO_4
0.54	31.01	3.55

Table 7: Mix proportion for concrete specimens (grade C30). Unit: kg/m^3.

Cement	Sand	Gravel (5–20 mm)	Water	Water reducing agent	Fly ash	Slag
262	767	1103	170	5.23	87	87

corrosion strengthening stage. This stage is followed by a stabilizing stage. Comparing with the concrete specimens in the IFT environment, the damage to the concrete specimens in the MFT environment is more seriously after 25 freeze-thaw cycles. K_c of the concrete specimens in the MFT environment decreases sharply from 25 to 50 freeze-thaw cycles and then decreases gradually as the freeze-thaw cycles increase. For example, K_c of the concrete specimens in the MFT environment is reduced by 59% after 150 freeze-thaw cycles, whereas for the concrete specimens in the IFT environment is reduced by 38%. Hence, the reduction in K_c of the concrete specimens in the MFT environment is 21% more than that in the IFT environment. From the results of the mass loss, E_r and K_c of the concrete specimens, they all show that the degree of damage of the concrete specimens in the MFT environment is more serious than that in the IFT environment. Therefore, when concrete is to be subjected to freeze-thaw cycles and multisalt solution attack, it is recommended to place concrete in a multisalt erosion environment for three months prior to freezing.

3.5. Analysis of Microstructure of Concrete Specimens

3.5.1. Analysis of Microstructure Using SEM and EDS. Figure 6 shows the SEM images of the deteriorated part of the concrete specimen in the IFT environment subjected to the multisalt solution attack and freeze-thaw cycles from 0 to 125. Figure 6(a) shows the microstructure of the concrete specimen attacked by the multisalt solution after 90 days. Before the 90 days, there were no freeze-thaw cycles, and the concrete microstructure is quite compact. As shown in Figure 6(a), the corrosion products of ettringite are formed inside the concrete; however, there are no microcracks. This may be attributed to the corrosion products of ettringite integrate with the concrete. Figure 6(c) shows the microstructure of the concrete in the IFT environment. It can be seen that there are several microcracks and the maximum width of the microcracks is approximately 0.8 μm. With the increase in the freeze-thaw cycles, for the concrete specimen in the IFT environment, the maximum width of the microcracks increases gradually, and large pores have a loose structure (Figure 6(e)).

Figure 7 shows the microstructure of the concrete specimen in the MFT environment. Before the freeze-thaw cycles, the SEM microscopic analysis shows that the concrete microstructure is quite compact because of the C-S-H dispersed well in the concrete (Figure 7(a)). After 25 freeze-thaw cycles, there are several voids in the concrete, as shown in Figure 7(b). With the increase in the freeze-thaw cycles, several corrosion products formed as indicated by the arrows in Figure 7(c). With the further increase in the freeze-thaw cycles, the voids became larger; thus, more corrosion products entered the interior of the concrete (Figure 7(d)). Therefore, they interacted and promoted each other. The maximum width of some microcracks is approximately 3.0 mm (Figure 7(e)), which is wider than that for the concrete specimen in the IFT environment.

The reason for the wider microcracks in the concrete specimen in the IFT environment may be attributed to the immersion of the concrete specimen in the multisalt solution for a long time before freezing. The advantage is that the chloride ions in the multisalt solution have strong penetration ability; they enter into the concrete to reduce the freezing point, prevent the invasion of sulfate ions, and reduce the corrosion production of ettringite, thereby improving its corrosion resistance performance. The disadvantage is that the concrete specimen in the IFT environment is easily eroded when subjected to the multisalt solution attack after demolition. However, the concrete specimen in the MFT environment has been immersed in the multisalt solution for only 28 days before freezing. In the MFT case, before 75 freeze–thaw cycles, due to the filling of corrosive products in a short period of time, the strength of concrete will increase; however, with the increase of corrosive ion concentration, especially sulfate ion concentration, excessive ettringite which are corrosive products will expand inside the concrete. When the expansion stress exceeds the tensile strength of concrete, the concrete will be damaged. In contrast, in the IFT case, before 75 freeze–thaw cycles, due to the filling of corrosive products in the curing time (90 d), corrosive products are integrated with the concrete [25], there are relatively few pores in concrete, and no more corrosive products enter the concrete; therefore, the damage is less. Therefore, the damage to the concrete specimen subjected to the freeze-thaw cycles is more serious than that subjected to the multisalt solution attack. In general, the degree of damage of the concrete specimen in the IFT environment is smaller than that in the MFT environment.

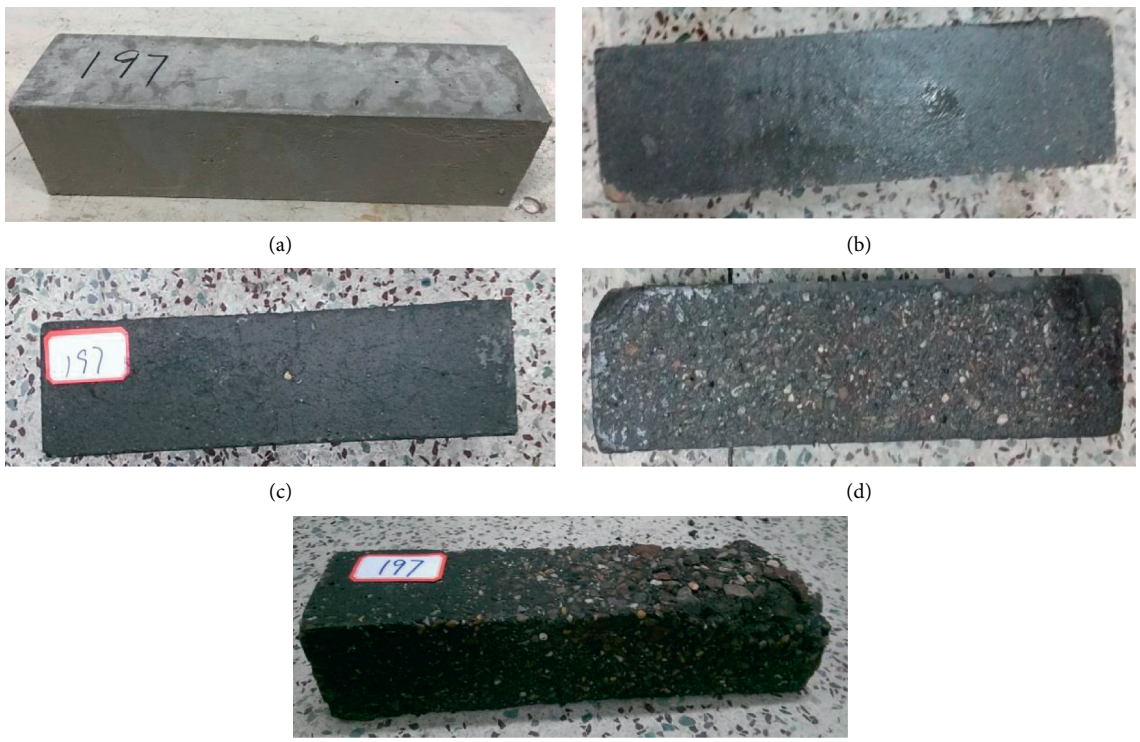

(a) (b) (c) (d) (e)

Figure 1: Typical failure modes of the concrete in the IFT environment. (a) 0 freeze-thaw cycles; (b) 25 freeze-thaw cycles; (c) 50 freeze-thaw cycles; (d) 75 freeze-thaw cycles; and (e) 125 freeze-thaw cycles.

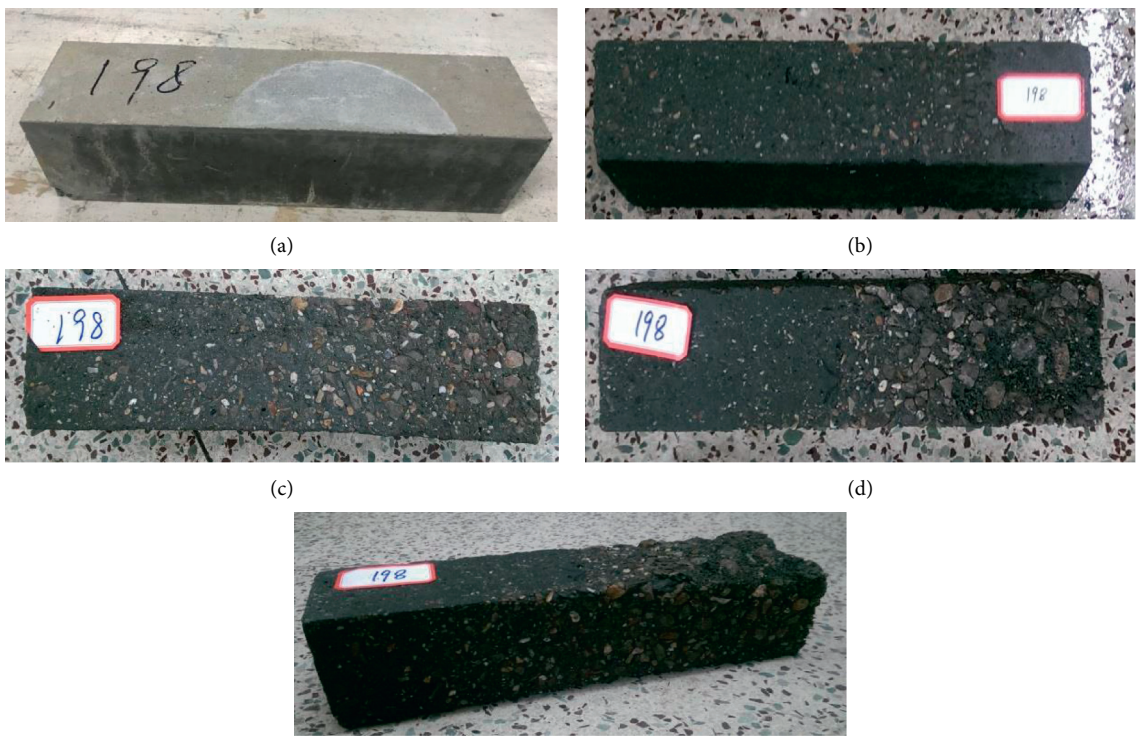

(a) (b) (c) (d) (e)

Figure 2: Typical failure modes of the concrete in the MFT environment. (a) 0 freeze-thaw cycles; (b) 25 freeze-thaw cycles; (c) 50 freeze-thaw cycles; (d) 75 freeze-thaw cycles; and (e) 100 freeze-thaw cycles.

Table 8: Visual assessment[a] of specimens' deterioration in concrete specimens.

Environment	Freeze–thaw cycles					
	0	25	50	75	100	125
IFT	0	1	2	3	b	4
MFT	0	1	3	4	5	—

[a]Deterioration scale; b: no test was carried out due to damaged experimental apparatus; 0: no visible deterioration; 1: some deterioration at corners; 2: deterioration at corners and cracking along the edges; 3: bulge of surfaces; 4: extensive spalling; and 5: complete damage.

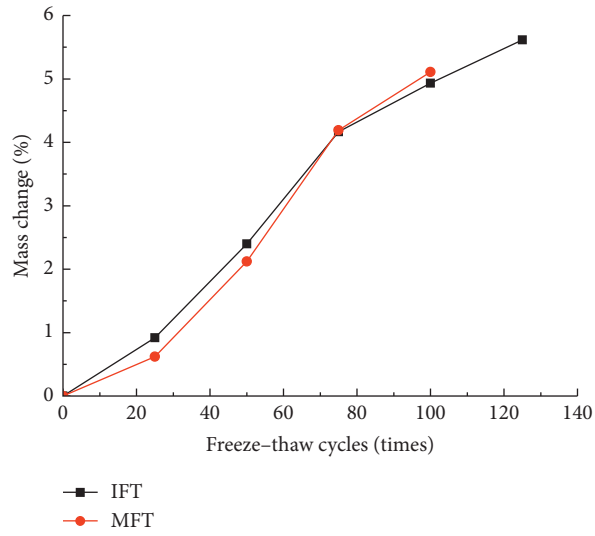

Figure 3: Variations of relative mass change of concrete specimens with freeze–thaw cycles in IFT and MFT environments.

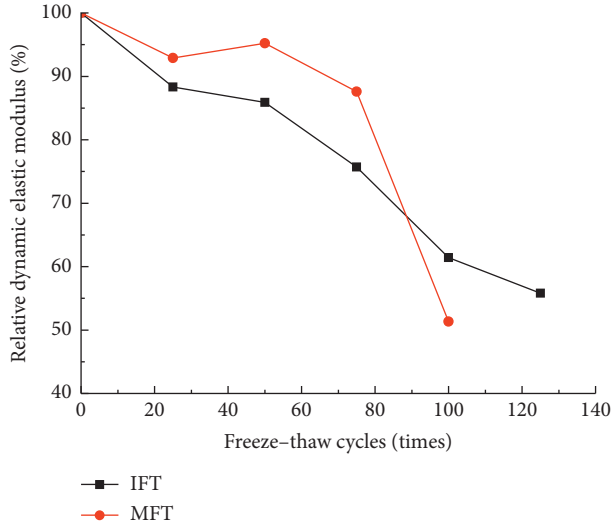

Figure 4: Variations of relative dynamic elastic modulus of concrete specimens with freeze–thaw cycles in IFT and MFT environments.

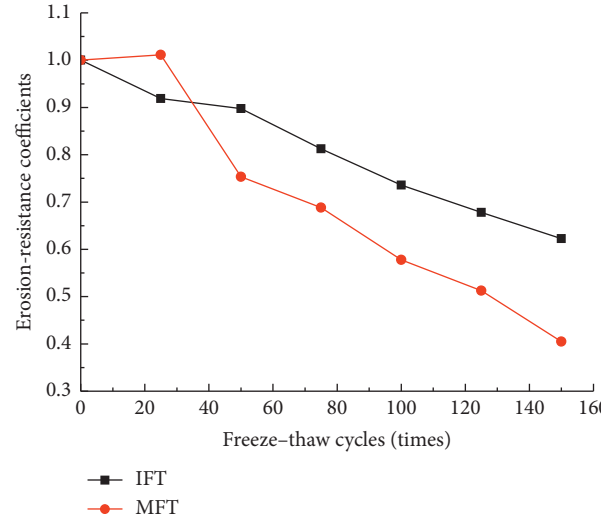

Figure 5: Variations of erosion-resistance coefficient of concrete specimens with freeze–thaw cycles in IFT and MFT environments.

3.5.2. Analysis of Microstructure Using MIP. Since pore structure directly affects the performance and durability of concrete, it is an important part of microstructure of concrete [33]. Figure 8 and Table 9 show that the internal pore size of the concrete specimen has changed significantly after two freeze-thaw environments, in both MFT and IFT. The average pore size, most probable pore size, median pore

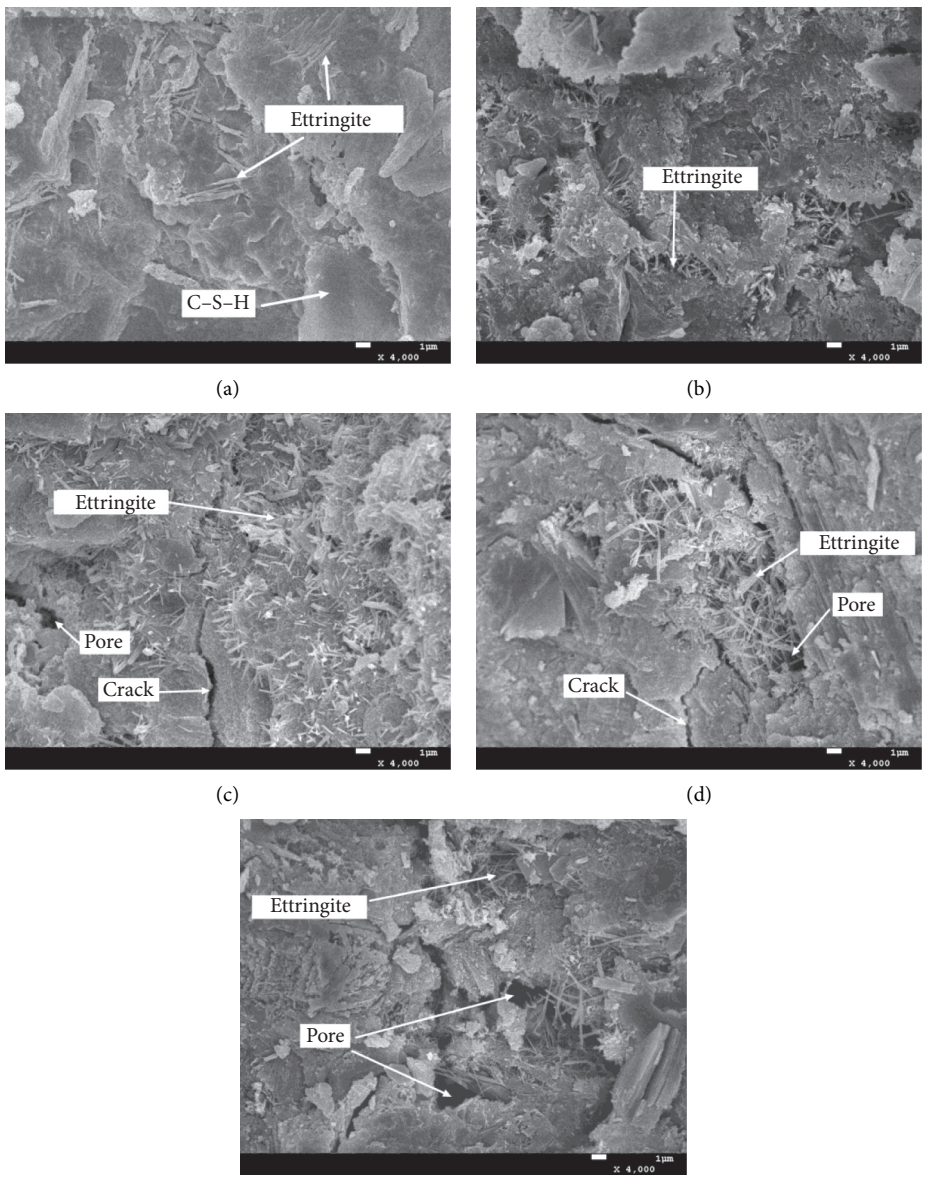

Figure 6: Microstructure of the concrete in the IFT environment. (a) 0 freeze-thaw cycles; (b) 25 freeze-thaw cycles; (c) 50 freeze-thaw cycles; (d) 75 freeze-thaw cycles; and (e) 125 freeze-thaw cycles.

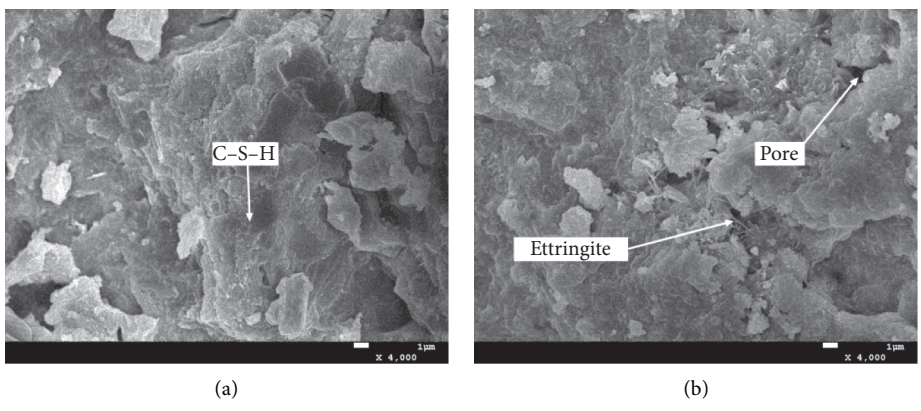

Figure 7: Continued.

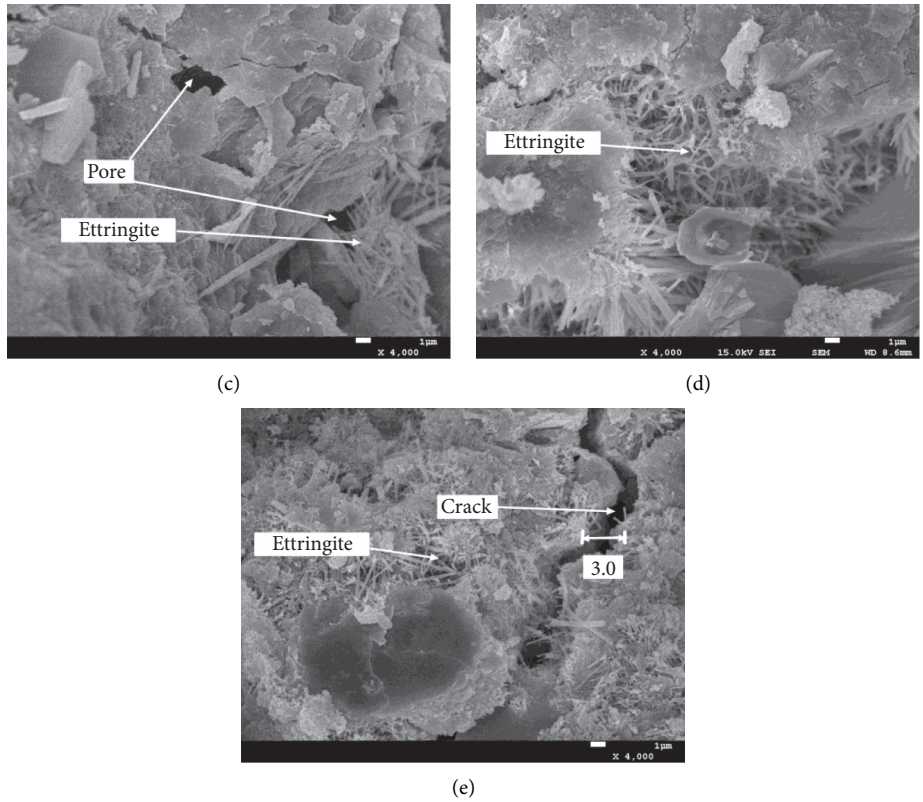

Figure 7: Microstructure of the concrete in the MFT environment. (a) 0 freeze-thaw cycles; (b) 25 freeze-thaw cycles; (c) 50 freeze-thaw cycles; (d) 75 freeze-thaw cycles; and (e) 100 freeze-thaw cycles.

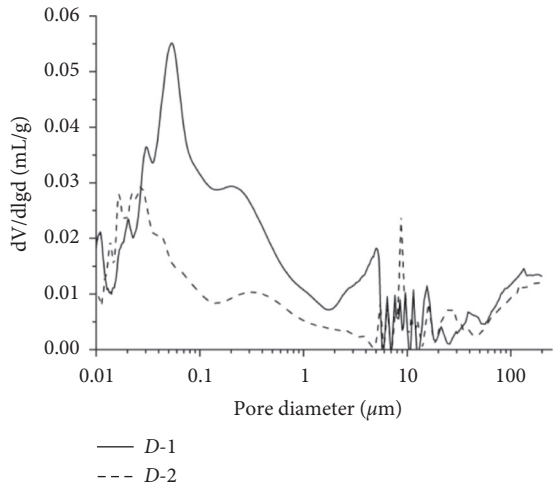

Figure 8: Pore size distributions of sample *D*-1 and *D*-2.

size, porosity, and total pore volume of the concrete specimen in the IFT environment subjected to 100 freeze-thaw cycles are all smaller than those of the concrete specimen in the MFT environment subjected to 125 freeze-thaw cycles. Wu et al. [34] found that, based on the classification of the pore size of concrete, smaller than 50 nm is harmless pore, equals 50–100 nm is harmful pore, and bigger than 100 nm is much harmful pore; the pore size distributions of the concrete specimens in the IFT and MFT environments are shown in Table 9.

From the overall pore size distribution, the proportions of the pore within the sizes of $d \leq 50$ nm, $50\text{ nm} \leq d \leq 100$ nm, and $d \geq 100$ nm for the concrete specimen in the MFT environment are 32.0%, 16.2%, and 51.8%, respectively, whereas for the concrete specimen in the IFT environment are 45.3%, 9.2%, and 45.5%, respectively. Although the

Table 9: Pore size distributions of concrete specimens in IFT and MFT environments.

Specimen	Mean pore D (nm)	Mode pore D (nm)	Median pore D (nm)	Total porosity (by volume) (%)	Total pore volume (10^{-2}·ml·g^{-1})	Pore volume (%)		
						$d \le 50$ nm	50 nm $\le d \le$ 100 nm	$d \ge 100$ nm
D-1	35.5	53.9	113.0	16.7	8.1	32.0	16.2	51.8
D-2	24.6	27.4	68.3	10.9	4.7	45.3	9.2	45.5

D-1 is the specimen of concrete in the MFT environment subjected to 100 freeze-thaw cycles, and D-2 is the specimen of concrete in the IFT environment subjected to 125 freeze-thaw cycles.

proportion of the pores within the size ($d \ge 100$ nm) for the concrete specimen in the MFT environment is similar to that for the concrete specimen in the IFT environment, the average pore size, median pore size, and porosity for the concrete specimen in the MFT environment are 1.44, 1.65, and 1.53 higher than that for the concrete specimen in the IFT environment, respectively. This is an indication that the damage to the concrete specimen in the MFT environment is more serious than that to the concrete specimen in the IFT environment. For the most probable aperture and total pore volume of the two concrete specimens, the difference is larger, where the value for the concrete specimen in the MFT environment is almost twice as large as for the concrete specimen in the IFT environment (Table 9). In summary, the deterioration process of concrete is the process of increasing the number of macropores, decreasing the number of micropores, and gradual expansion of microcracks.

4. Conclusions

This study investigates the damage to concrete subjected to the two freeze–thaw environments (i.e., maintenance freeze-thaw environment and immersion freeze-thaw environment) attack. The conclusions are as follows.

On the basis of the erosion-resistance coefficients, mass change, relative dynamic elastic modulus, and microstructure of the concrete, the damage to the concrete in the MFT environment is more serious than that in the IFT environment.

After 150 freeze-thaw cycles, the erosion-resistance coefficient of the concrete in the MFT environment decreases by 59%, whereas that of the concrete in the IFT environment decreases by 38%. The decrease in the erosion-resistance coefficient of the concrete in the MFT environment is therefore 21% more than that of the concrete in the IFT environment.

The analyses of the microstructure of concrete show that, under the action of various environmental factors, the corrosion damage to concrete is caused by the accumulated damage caused by pore development, microcrack development, and penetration.

Data Availability

The data used to support the findings of this study are included in the article.

Conflicts of Interest

The authors declare that they have no conflicts of interest regarding the publication of this paper.

Acknowledgments

The authors would like to express their gratitude to the National Natural Science Foundation of China (51779095 and 51679092) and the Science Technology Innovation Talents in Universities of Henan Province (20HASTIT013).

References

[1] P. Zhang, Q.-F. Li, J. Wang, Y. Shi, and Y.-F. Ling, "Effect of PVA fiber on durability of cementitious composite containing nano-SiO_2," *Nanotechnology Reviews*, vol. 8, no. 1, pp. 116–127, 2019.

[2] P. Zhang, Y. Zheng, K. Wang, and J. Zhang, "A review on properties of fresh and hardened geopolymer mortar," *Composites Part B: Engineering*, vol. 152, pp. 79–95, 2018.

[3] H. Ma, H. Yu, C. Li, Y. Tan, W. Cao, and B. Da, "Freeze-thaw damage to high-performance concrete with synthetic fibre and fly ash due to ethylene glycol deicer," *Construction and Building Materials*, vol. 187, no. 187, pp. 197–204, 2018.

[4] Z. Zhou and P. Qiao, "Durability of ultra-high performance concrete in tension under cold weather conditions," *Cement and Concrete Composites*, vol. 94, no. 94, pp. 94–106, 2018.

[5] K. W. Liu, D. S. Sun, A. G. Wang, G. Zhang, and J. Tang, "Long-term performance of blended cement paste containing fly ash against sodium sulfate attack," *Journal of Materials in Civil Engineering*, vol. 30, no. 12, pp. 1–10, Article ID 04018309, 2018.

[6] P. Zhang, Q. F. Li, Y. Z. Chen, Y. Shi, and Y.-F. Ling, "Durability of steel fiber-reinforced concrete containing SiO_2 nano-particles," *Materials*, vol. 12, no. 13, pp. 1–18, Article ID 2184, 2019.

[7] D. P. Forgeron and J. F. Trottier, "Evaluating the effects of simultaneous freezing and thawing and flexural fatigue loading cycles on the fracture properties of FRC," in *High Performance Structures and Materials Proceedings No. 2*, W. P. De Wilde and C. A. Brebbia, Eds., WIT Press, Chilworth, SO, USA, 2004.

[8] J. F. Trottier and D. P. Forgeron, "Cumulative effects of flexural fatigue loading and freezing and thawing cycles on the flexural toughness of fiber reinforced concrete," in *Concrete under Severe Conditons Proceedings No. 3*, N. Banthia, K. Sakai, and O. E. Gjφrv, Eds., Routledge Press, Abingdon, UK, 2011.

[9] B. Diao, J. Zhang, Y. H. Ye, and S. Cheng, "Effects of freeze-thaw cycles and seawater corrosion on the behavior of reinforced air-entrained concrete beams with persistent loads," *Journal of Cold Regions Engineering*, vol. 27, no. 1, pp. 44–53, 2013.

[10] F. Y. Gong, E. Sicat, D. W. Zhang, and T. Ueda, "Stress analysis for concrete materials under multiple freeze-thaw cycles," *Journal of Advanced Concrete Technology*, vol. 13, no. 3, pp. 124–134, 2015.

[11] B. Diao, Y. Sun, S. H. Cheng, and Y. Ye, "Effects of mixed corrosion, freeze-thaw cycles, and persistent loads on

behavior of reinforced concrete beams," *Journal of Cold Regions Engineering*, vol. 25, no. 1, pp. 37–52, 2011.

[12] B. Amini and S. S. Tehrani, "Combined effects of saltwater and water flow on deterioration of concrete under freeze-thaw cycles," *Journal of Cold Regions Engineering*, vol. 25, no. 4, pp. 145–161, 2011.

[13] A. E. Richardson, K. A. Coventry, and G. Ward, "Freeze/thaw protection of concrete with optimum rubber crumb content," *Journal of Cleaner Production*, vol. 23, no. 1, pp. 96–103, 2012.

[14] J. Yuan, Y. Liu, H. Li, and B. Zhang, "Experimental investigation of the variation of concrete pores under the action of freeze-thaw cycles by using X-Ray CT," *Advances in Materials Science and Engineering*, vol. 2014, Article ID 571357, 11 pages, 2014.

[15] Z. Wang, Q. Zeng, Y. Wu, L. Wang, Y. Yao, and K. Li, "Relative humidity and deterioration of concrete under freeze-thaw load," *Construction and Building Materials*, vol. 62, pp. 18–27, 2014.

[16] H. S. Shang, T. H. Yi, and Y. P. Song, "Behavior of plain concrete of a high water-cement ratio after freeze-thaw cycles," *Materials*, vol. 5, no. 9, pp. 1698–1707, 2012.

[17] J. Ranz, S. Aparicio, H. Romero, M. Casati, M. Molero, and M. González, "Monitoring of freeze-thaw cycles in concrete using embedded sensors and ultrasonic imaging," *Sensors*, vol. 14, no. 2, pp. 2280–2304, 2014.

[18] W. T. Li, M. Pour-Ghaz, J. Castro, and J. Weiss, "Water absorption and critical degree of saturation relating to freeze-thaw damage in concrete pavement joints," *Journal of Materials in Civil Engineering*, vol. 24, no. 3, pp. 299–307, 2012.

[19] A. E. Richardson, K. A. Coventry, and S. Wilkinson, "Freeze/thaw durability of concrete with synthetic fibre additions," *Cold Regions Science and Technology*, vol. 83-84, no. 83, pp. 49–56, 2012.

[20] P. Zhang, Y. Zheng, K. Wang, and K. Zhang, "Combined influence of nano-$CaCO_3$ and polyvinyl alcohol fibers on fresh and mechanical performance of concrete incorporating fly ash," *Structural Concrete*, vol. 21, no. 2, pp. 724–734, 2019.

[21] P. Zhang, Z. Gao, J. Wang, J. Guo, S. Hu, and Y. Ling, "Properties of fresh and hardened fly ash/slag based geopolymer concrete: a review," *Journal of Cleaner Production*, vol. 270, Article ID 122389, 2020.

[22] P. Zhang, K. Wang, J. Wang, J. Guo, S. Hu, and Y. Ling, "Mechanical properties and prediction of fracture parameters of geopolymer/alkali-activated mortar modified with PVA fiber and nano-SiO_2," *Ceramics International*, vol. 46, no. 12, pp. 20027–20037, 2020.

[23] G. F. Li and X. D. Shen, "A study of the durability of aeolian sand powder concrete under the coupling effects of freeze-–thaw and dry–wet conditions," *JOM*, vol. 71, no. 6, pp. 1962–1974, 2019.

[24] X. P. Su and Q. Wang, "Corrosion damage of concrete under multi-salt soaking, freezing-thawing and dry-wet cycles," *Journal of Jilin University (Engineering and Technology Edition)*, vol. 1, no. 1, pp. 112–120, 2015, (in Chinese).

[25] X. H. Yao, Z. J. Feng, F. C. Wang et al., "Property of multiple admixture concrete in multi-salt soaking under wetting-drying and freezing-thawing cycles," *Acta Compositae Sinica*, vol. 35, no. 3, pp. 690–698, 2018, (in Chinese).

[26] X. H. Yao, Z. J. Feng, F. C. Wang et al., "Experiment on erosion-resistance of highway bridge pile foundation material under salt marshes environment," *Journal of Chang'an University (Natural Science Edition)*, vol. 38, no. 1, pp. 49–58, 2018, (in Chinese).

[27] X. D. Shi, Y. Q. Li, L. Qian et al., "Experimental Study on elastic modulus of concrete undergoing freeze-thaw cycle action with different ultralow temperature ranges," *Engineering Mechanics*, vol. 36, no. 8, pp. 106–113, 2019, (in Chinese).

[28] Z. G. Yin, K. Zhang, W. Fan et al., "Experimental study on the durability of recycled aggregate pervious concrete under different freeze-thaw media conditions," *Bulletin of the Chinese Ceramic Society*, vol. 38, no. 7, pp. 2137–2143, 2019, (in Chinese).

[29] G. Xu, C. Gong, J. Liu et al., "Correlation between water freeze-thaw resistance and salt freeze-thaw cycle of concrete," *Journal of Building Materials*, vol. 1–10, 2020 (in Chinese).

[30] Y. R. Zhao, X. Q. Fan, L. Q. Wang et al., "Attenuation model of mechanical properties of concrete under different freezing and thawing," *Acta Materiae Compositae Sinica*, vol. 34, no. 2, pp. 463–470, 2017, (in Chinese).

[31] S. W. Hu and Y. Wang, "Experimental study on double-K fracture toughness of concrete in different freezing and thawing modes," *Hydro-Science and Engineering*, vol. 2, pp. 90–96, 2018, (in Chinese).

[32] X. H. Yao, *Mechanics Properties and Safety Evaluation of Highway Bridge Pile in Alpine Salt marshes*, Chang'an University, Xi'an, China, 2018, (in Chinese).

[33] Y. Xiong, D. Wu, and F. A. Liu, "Experimental study on realkalization repair of concrete compressive strength after high-temperature based on microstructure analysis," *Engineering Mechanics*, vol. 6, no. 6, pp. 205–211, 2013, (in Chinese).

[34] Z. W. Wu and H. Z Lian, *High Performance Concrete*, China Railway Publishing House, Beijing, China, 1999, (in Chinese).